Changes in lead and zinc lability during weathering-induced acidification of desert mine tailings: Coupling chemical and micro-scale analyses

Sarah M. Hayes[a], **Scott A. White**[a], **Thomas L. Thompson**[b], **Raina M. Maier**[a], and **Jon Chorover**[a],[*]

[a]Department of Soil, Water and Environmental Science, University of Arizona, Tucson, AZ 85721-0038, USA.

[b]Department of Plant and Soil Science, Texas Tech University, Lubbock, TX 79409, USA.

Abstract

Desert mine tailings may accumulate toxic metals in the near surface centimeters because of low water through-flux rates. Along with other constraints, metal toxicity precludes natural plant colonization even over decadal time scales. Since unconsolidated particles can be subjected to transport by wind and water erosion, potentially resulting in direct human and ecosystem exposure, there is a need to know how the lability and form of metals change in the tailings weathering environment. A combination of chemical extractions, X-ray diffraction, micro-X-ray fluorescence spectroscopy, and micro-Raman spectroscopy were employed to study Pb and Zn contamination in surficial arid mine tailings from the Arizona Klondyke State Superfund Site. Initial site characterization indicated a wide range in pH (2.5 to 8.0) in the surficial tailings pile. Ligand-promoted (DTPA) extractions, used to assess plant-available metal pools, showed decreasing available Zn and Mn with progressive tailings acidification. Aluminum shows the inverse trend, and Pb and Fe show more complex pH dependence. Since the tailings derive from a common source and parent mineralogy, it is presumed that variations in pH and "bioavailable" metal concentrations result from associated variation in particle-scale geochemistry. Four sub-samples, ranging in pH from 2.6 to 5.4, were subjected to further characterization to elucidate micro-scale controls on metal mobility. With acidification, total Pb (ranging from $5 – 13$ g kg^{-1}) was increasingly associated with Fe and S in plumbojarosite aggregates. For Zn, both total ($0.4 – 6$ g kg^{-1}) and labile fractions decreased with decreasing pH. Zinc was found to be primarily associated with the secondary Mn phases manjiroite and chalcophanite. The results suggest that progressive tailings acidification diminishes the overall lability of the total Pb and Zn pools.

1. Introduction

Because of low water through-flux combined with episodic wetting and drying, desert sulfide mine tailings may accumulate toxic metals in weathering products, such as sulfate salts and mixed valence hydrous oxides (Jambor, 1994). During rainwater infiltration, solid phase dissolution releases metals to solution along a reaction path that depends on mineral solubility dynamics (Blowes et al., 2005). Sulfide mineral oxidation results in formation of sulfate solids,

including gypsum and jarosite, early in diagenesis, and this incongruent dissolution controls dissolved SO_4 concentration (McGregor et al., 1998; Johnson et al., 2000; Romero et al., 2007). As shown by Jambor and co-workers, protons released from sulfide oxidation are consumed through a consecutive series of gangue mineral dissolution reactions (first calcite, then silicates, then oxides), which, as a result of the relative rates of sulfide and gangue mineral weathering reactions, leads to a progressive tailings acidification (Jambor, 1994; Blowes et al., 2005).

In humid climates, soluble sulfate minerals (e.g., gypsum) and poorly-crystalline oxides may not accumulate because of extensive leaching (eg. Davis et al., 1993; O'Day et al., 1998; Jeong and Lee, 2003; Schuwirth et al., 2007). However, in arid or semi-arid regions, soluble minerals and acidity persist near the weathering front because of a lack of fresh water, as has been shown for Cu-containing pyrite tailings in the Rio Tinto region of Spain (Hudson-Edwards et al., 1999), in arid regions of Chile (Dold and Fontbote, 2001) and southeastern Spain (Wray, 1998; Navarro et al., 2004). Associated weathering reactions can potentially sequester metals into neo-formed clay minerals, sulfate solids and (oxyhydr)oxides of Fe, Mn and Al (Jambor, 1994; Hudson-Edwards et al., 1996).

As a result of the co-occurrence of high bio-available metal concentrations and low water availability (as well as low pH, high dissolved salts, and poor soil structure), many desert mine tailings are inhospitable for colonization by plants, which could physically stabilize tailings (Mendez and Maier, 2008). This is mirrored by the resident microbial communities that tend to be depleted in heterotrophic relative to autotrophic biomass (Mendez et al., 2008). Activities of the S and Fe oxidizing organisms promote acidification of tailings piles, which further hinders plant establishment. The lack of plant colonization has human health implications because metal-containing tailings particles, which are then extremely vulnerable to wind and water erosion, can be mobilized to expose nearby communities and ecosystems (Plumlee and Ziegler, 2005).

Since surficial tailings may contain high concentrations of toxic metals (e.g., Pb, Cd, Zn), it is necessary to know how "labile" these particulate metal pools are, including the ease with which they are transferred between the solid and solution phases (Schaider et al., 2007). This is particularly important since links between metal lability and toxicity have been clearly established (Maiz et al., 2000; Plumlee and Ziegler, 2005; Finzgar et al., 2007; Alvarenga et al., 2008). Selective chemical extractions of geological samples, including tailings, provide quantitative indices of contaminant lability (Tessier et al., 1979; Sondag, 1981; Ribet et al., 1995; Dold, 2003b). But they have also been criticized for non-specificity, incomplete dissolution of target phases, and potential for artifacts (Hall et al., 1996; McCarty et al., 1998; Calmano et al., 2001). This is because it is difficult to interpret quantitative indices of element mobility, such as those provided by chemical extractions, without having additional micro-and/or molecular-scale information on the metal-containing particles themselves (Schulze, 1994; Dold, 2003a; Choi et al., 2005).

Therefore, in the present work, the aurhors sought to combine chemical extractions of bulk tailings media with bulk and micro-focused spectroscopy of particles within the mineral assemblage in order to better understand the specific phases controlling metal sequestration and release. The lability of metals was assessed quantitatively using chemical extractions. For the purposes of the current work, the "labile fraction" is defined as that portion of the total solid-phase metal concentration that is extracted by diethylenetriaminepentaacetic acid (DTPA) in a single extraction step or, alternatively, by the water soluble plus exchangeable fractions removed in the first two steps of a sequential extraction scheme described more fully below. While such extractions tentatively assign metals to target phases undergoing solubilization, additional analytical methods were employed on the residual solids for direct

confirmation. Grain-scale, mineral-metal associations were detected directly using differential X-ray diffraction (Schulze, 1994), and micro-focused methods, including micro-X-ray fluorescence spectroscopy (Manceau et al., 2002; Bernaus et al., 2006; Chorover et al., 2008) and micro-Raman spectroscopy (Skoog et al., 1998). Micro-Raman spectroscopy can detect micrometer sized particles of both crystalline and poorly-crystalline forms, even when the latter are amorphous to X-ray diffraction (XRD) (Filippi et al., 2007; Courtin-Nomade et al., 2008). Despite its potential utility, there have been few prior applications of micro-Raman spectroscopy to mineral identification in mine tailings (Stefaniak et al., 2006).

The objective of the current study is to relate particle composition to contaminant (Pb and Zn) lability in surficial mine tailings of the Arizona Department of Environmental Quality (DEQ) Klondyke State Superfund Site in southeasern Arizona. The Klondyke tailings were selected for study because they have been weathering in a semi-arid desert environment since their deposition more than 50 a ago. The microbial community composition of these tailings has been well studied (Mendez et al., 2008); and it shows a predominance of S and Fe oxidizers and very low heterotrophic bacterial counts. The latter is due, in part, to the fact that the tailings remain uncolonized by plants. Since natural plant colonization is rare in desert mine tailings, the authors' group is researching economical, biogeochemical strategies for phytostabilization of these systems (Grandlic et al., 2008). High concentrations of metals – up to 15 g kg^{-1} Pb and 5 g kg^{-1} Zn – remain in surficial tailings in a wide range of pH environments (2.3 to 8.0), thereby serving as a principal source of contamination to an adjacent riparian ecosystem.

2. Site description

The Klondyke Superfund Site (ID# 1236) is located in Graham County, Arizona (N32 50.990 W110 20.552) within the Aravaipa Creek watershed. Lead and Zn sulfide ore was mined in the region from the 1870s to the mid 1900s. A flotation mill, capable of concentrating up to 100 tons of ore per day, was built in 1942, and served the Head Center and Iron Cap mines until closure in 1958. Klondyke tailings derive from its operation from 1948 to 1958 (Simons, 1964).

The ore bodies of both mines are low temperature hydrothermal deposits containing quartz, johannsenite, calcite and sulfides found in low angle faults either between bedding plains of the Horquilla limestone or between the Horquilla limestone and an overlying volcanic layer (Simons, 1964). The Head Center and Iron Cap ores contained up to (in g kg^{-1}) 380 Pb and 60 Zn, and 190 Pb and 350 Zn, respectively. The sulfide mineral composition of the deposited material, after metal extraction, was sphalerite (ZnS), galena (PbS), pyrite (FeS$_2$), and chalcopyrite (CuFeS$_2$) (Scott, 1988; Goodwin, 2000). From preliminary assessments (Tummala and Humble, 1998; Goodwin, 2000), the Arizona DEQ determined that the tailings exceed acceptable soil concentration levels for several toxic metals, including Pb, and therefore require remediation. The current project was motivated, in part, by a need to assess the potential for phytostabilization as a means for remediation.

3, Materials and methods

3.1 Field-Scale Variation in DTPA Extractable Metals

In a pre-screening of bio-available metal pools, the approximately 11,000 m^2 pile was sampled with precise locations documented by GPS in 3 transects, each comprising 4 or 5 sampling points ca. 30 m apart over the entire top of the tailings pile to obtain 13 samples from each of two depths (0–30 cm and 30–60 cm). Each sample was air-dried, sieved to obtain the fine earth (< 2 mm) fraction and then subjected to (i) measurement of pH and electrical conductivity (by electrode on aqueous solutions obtained from 1:1 mass ratio of tailings to 18 MΩ deionized water reacted for 1 h). The diethylenetriaminepentaacetic acid (DTPA) extraction, which

provides a quantitative measure of plant-available metals (Amacher, 1996), was performed in triplicate for each sampling location. For each replicate, 10.0 g tailings and 20.0 g DTPA solution were combined, shaken vigorously for 2 h then centrifuged at 43,870 relative centrifugal force (RCF) and filtered (0.2 µm) prior to solution phase analysis by inductively coupled plasma mass spectrometry (ICP-MS, Perkin Elmer SCIEX Elan DRC II, Shelton, CT).

Following the initial screening, 4 samples ($T_{2.6}$, $T_{3.9}$, $T_{4.2}$, and $T_{5.4}$ with subscripts denoting the saturated paste pH values) were selected for further detailed study using the methods discussed below. These samples have been referred to in previous publications as K4, T1, K6, and T2, respectively (Grandlic et al., 2008; Mendez et al., 2007; Vazquez-Ortega et al., 2009), and were collected from depths of 28–53 cm, 0–30 cm, 21–42 cm, and 0–30 cm. As with the screening samples, upon return to the laboratory, the 4 tailings were sieved to obtain the < 2 mm fraction, which was air dried for a period of 2 weeks, and then stored in covered, 5-gallon (19 L) containers at room temperature.

3.2. Bulk Physical, Mineralogical and Chemical haracterizations

3.2.1. Particle size separation and analysis—Particle size separation was performed in triplicate using the pipette sedimentation method (Burt, 2004). The tailings were dispersed in 50 mL of 0.058 M sodium hexametaphosphate $(NaPO_3)_6$ and 0.075 M Na_2CO_3 solution at low speed on a reciprocal shaker for 24 h prior to removal of the sand fraction by sieving. The silt and clay were transferred into a 1 L graduated cylinder for sedimentation, and the clay content was sampled after 3 h 38 min at 23°C. After further settling, clays were decanted and the silt fraction was washed in pH 9.5, 1.0 mM Na_2CO_3 solution, and then pelleted by centrifugation. The clay-containing supernatant suspension was added to the decanted clays and flocculated using NaCl. The clay suspension was then desalted by dialysis (VWR, Spectrapor MWCO 12–14k, 25225-260). A portion of the clay suspension was used for creating oriented clay slides for XRD analysis, the remainder was freeze-dried.

3.2.2. Particle digestion and total elemental analysis—Duplicate composite samples (11 g) of each tailings material were subjected to total elemental analysis (Activation Laboratories, Ontario, Canada). Methods included neutron activation analysis, and total HF-HNO_3-HCl-$HClO_4$ digestion, lithium metaborate/tetraborate fusion followed by HNO_3 digestion, prior to solution phase analysis by ICP-MS. Triplicate determinations of total and inorganic C and total nitrogen were performed on the solid phase using a Shimadzu TOC-VCSH analyzer (Columbia, MD) with a solid state module (SSM-5000A).

3.2.3. Bulk and clay mineral composition—Crystalline mineral composition of the tailings was determined by a combination of synchrotron-radiation (SR) and laboratory-based X-ray diffraction (XRD). SR-XRD was conducted at the Stanford Synchrotron Radiation Laboratory (SSRL) on Beamline 11-3, operating at ~12,700 eV, using a Mar detector with a 345 mm radius with 100 µm pixels. Ring potential at SSRL was 2 GeV, and current varied from 100 to ~40 mA during data collection. Random powder diffraction patterns of bulk tailings were collected in transmission mode with the sample encased in Scotch Magic matte finish tape and placed 150 mm from the detector, corresponding to a d-spacing range of 1.47 to 48 Å. The sample was scanned over a 1 mm^2 section normal to the beam in 64 points (8×8 grid). Five or more scans were collected for each sample for subsequent addition to avoid detector saturation from the quartz peaks. Data were reduced using the Area Diffraction Machine software with a mask covering the beamstop (Lande et al., 2007). The patterns were added, reduced, converted to Cu Kα scale, and analyzed using X'Pert software (X'Pert Highscore Plus, version 2.1b). Spectra were aligned to the quartz peak at 39.50 °2θ, and normalized to 50,000 counts for the same peak, assuming that all samples have roughly the same mass fraction of quartz. To image the peaks lost during the sequential extraction steps, the diffractograms were

analyzed using the differential pattern analysis method (Dold, 2003b). Diffractograms were aligned in X'Pert Pro by slightly adjusting the peak heights and position. Following pre- minus post- pattern subtraction, difference patterns were analyzed.

The tailings clay (< 2 µm) fraction was analyzed using laboratory-based XRD (Panalytical X'Pert PRO). The clay suspension from the particle size separation was used to create oriented clay slides (Jackson, 1985). Magnesium saturated clays were analyzed first, then again after their saturation with glycerol, and with formamide. Potassium saturated clays were analyzed at room temperature and after 1 h heat treatment at 100, 300 and 550 °C. Diffraction intensities were collected from 2 to 30 °2θ with a stepsize of 0.01 °2θ, and a dwell time of 2 s/step.

3.2.4. Aqueous extraction—The 4 tailings were extracted in triplicate in 50 mL PPCO centrifuge tubes at unit solid/solution mass ratio in ultrapure (18 MΩ) water. Samples were reacted for 24 h on an end-over-end mixer (10 rpm). The solution phase was separated by centrifugation at 43,870 RCF for 20 min and filtered (Acrodisk, 0.2 µm) before chemical analysis. Solution pH and EC were measured by electrode. Dissolved organic C and N were measured using a Shimadzu Total Carbon Analyzer (TOC-VCSH). Anions were measured by ion chromatography (Dionex Ion Chromatograph DX-500, Sunnyvale, CA) with an AS-11 column and a NaOH mobile phase. Metal(loid)s were measured by ICP-MS.

3.2.5. Cation exchange capacity—The tailings cation exchange capacity was measured using the method described by Sumner and Miller (1996), which is optimized for porous geomedia that contain soluble salts such as gypsum.

3.2.6. Sequential chemical extraction—A 6-step method developed for Cu mine tailings (Dold, 2003b) was used to measure the quantity of metals extracted into operationally-defined pools targeting specific phases. The procedure involved addition of 1.0 g of air-dried tailings to 50 mL Teflon centrifuge tubes in triplicate followed by the following reaction sequence: (i) 18MΩ water extraction (25°C, 1 h) that targets soluble salts such as gypsum, (ii) 1.0 M ammonium acetate (pH 4.5, 25°C, 2 h) that targets sorbed species, and calcite, (iii) 0.2 M ammonium oxalate (pH 3.0, 25°C, 2 h) that targets short-range-order Fe, Al and Mn (oxy) hydroxides and poorly-crystallized jarosites (referred to hereafter as "AAO 25°C"), (iv) 0.2 M ammonium oxalate (pH 3.0, 80°C, 2 h) that targets long-range-order Fe, Al, and Mn (oxy) hydroxides and well-crystallized jarosites (referred to hereafter as "AAO 80°C"), (v) 30–35% H_2O_2 in 1.0 M ammonium acetate (pH 4.5, 60°C, 2 h) that oxidizes organic matter and secondary supergene sulfides, (vi) 750 mg of $KClO_3$ and l5 mL 12 M HCl (25°C, 30 min) with 10 mL of 18 MΩ water added for dilution before centrifugation and decanting the supernatant prior to reacting pellets with 25mL of 4 M HNO_3 (90°C, 20 min) that targets primary sulfides. Triplicate samples of the residual solids were harvested after rinsing 3 times with ethanol, followed by freeze-drying and XRD and X-ray absorption spectroscopy analysis. After each step, the pellets were rinsed with 30 mL of 18 MΩ water, the combined supernatant and wash solutions were collected by centrifugation, filtered using a 0.2 µm Acrodisk filter, acidified to pH 2, and analyzed by ICP-MS for metal concentrations.

3.2.7. X-ray absorption spectroscopy—The freeze-dried solid phase harvested at each step during the sequential extraction was analyzed by Pb L_{III} edge extended X-ray absorption fine structure (EXAFS) spectroscopy at GSE-CARS beamline 13-BM at the Advanced Photon Source (Argonne National Laboratory, IL). Measurements were made at room temperature using a 13-element Ge detector. Further investigation of the unextracted and post-AAO80°C extracted pellets were performed using an Oxford cryostat operating at 4K on beamline 11-2 at SSRL with the Si 220 Φ=0 monochromator crystal with a 32-element Ge detector. A minimum of 3 scans were collected in transmission for references and 10–15 scans were collected in fluorescence mode for samples. The spectra were analyzed using Sixpack (Webb,

2005) as described elsewhere (Hayes et al., 2009). Briefly, the spectra were calibrated to the Pb L_{III} edge (E_0=13,035 eV), averaged, and the EXAFS portions of the spectra were extracted prior to analysis by principle component analysis (PCA), and target transform analysis (TTA) (e.g., Scheinost et al., 2005). Simple two-component linear combination of reference standards were used to fit both the XANES and EXAFS regions for the data discussed here.

3.3. Grain Phase Identification and Elemental Associations

3.3.1. Preparation of thin sections—Thin sections were prepared using an epoxy impregnation procedure (Arai et al., 2003). Tailings were placed into a 50 mL beaker that was then gradually filled with EPOTEC 301-2FL epoxy while under vacuum to remove air bubbles. Embedded samples were cured for 3 days under vacuum before being sent to Spectrum Petrographics (Vancouver, WA), where they were thin sectioned to 30 µm, polished on both sides, and mounted on quartz slides.

3.3.2. X-ray fluorescence spectroscopy—X-ray fluorescence elemental mapping was performed on beamline 2–3 at SSRL using a Si220 Φ=0 monochromator crystal and a single element vortex detector. The scans were collected with 2.5 µm stepsize and a dwell time of 250 ms. The thin sections were placed directly in front of the X-ray beam (13050 eV), just above the Pb L_{III} absorption edge. The XRF maps were analyzed using SMATK (Webb, 2006). Each map is linearly scaled from lowest counts (black) to highest counts (white).

3.3.3. Micro-Raman spectroscopy—Micro-Raman spectroscopy was employed using a benchtop Nicolet Almega XR dispersive Raman instrument with either a 10× or 50× focusing objective for phase identification of the same particles mapped with XRF. Using the 10× objective, the 532 nm laser probes a 1 µm spot size. Spectra were collected using Omnic software (Thermo Scientific version 7.4, Madison, WI), and analyzed using Crystal Sleuth software by comparison to reference spectra in the RRUFF database (Downs, 2006).

4. Results

4.1 Tailings Physical-Chemical Properties

The initial samples were analyzed for pH, EC and DTPA extractable metals to assess trends in metal phyto-availability (Amacher, 1996) across the tailings pile. Contour plots of selected constituents based on data kriging demonstrate the large spatial distribution of pH and metals (Fig. 1). While the principal interest relates to the contaminants Zn and Pb, data are included on Al, Fe and Mn because these metals were found to show interesting bulk and particle scale relationships with the contaminant metals. The top row in Figure 1 shows chemical data for the 0–30 cm depth, whereas the bottom row depicts the same for the 30–60 cm depth. Extractable Mn and Zn in the surface and subsurface appear to follow linear trends in pH (Fig. 2 c,e), and also exhibit correlation with each other (Fig. 1 and Fig. 2g). Both Fe and Pb show weaker linear dependence on pH (Fig. 2d,f). DTPA extractable Al decreases with pH (Fig. 2b). There is no strong effect of sampling depth on the mass of metals extracted by DTPA at a given pH.

Based on these initial findings, it was speculated that variation in metal lability (as reflected in DTPA extractions) varies across the tailings because of variation in grain scale mineralogy and geochemistry. To test this, 4 samples were selected from the locations indicated in the pH plots of Figure 1, and subjected to detailed analysis. Certain baseline physical and chemical properties such as texture, organic C, total N, total S, and electrical conductivity, of the 4 samples selected for in-depth characterization (Table 1) were very similar, while the pH (2.6–5.4) varied significantly, suggesting that other chemical properties (e.g., metal lability) may likewise vary. All samples have a similar particle size distribution, ranging from 50–62% sand,

19–33% silt, and 8–11% clay by mass. The tailings all give rise to pore waters with high electrical conductivity (3.0 to 5.6 mS cm^{-1}), and low dissolved organic C and N. Solid phase inorganic C was below detection limit (< 66 mg kg^{-1}) for all but $T_{4.2}$ (590 mg kg^{-1}). Total elemental concentrations of the tailings are given for selected elements in Table 3.

4.2 Bulk and Clay Mineralogy

Several primary minerals (listed in bold font in Table 2) were identified in the tailings using XRD. The dominant diffraction intensities derive from primary framework silicates: quartz and orthoclase (Fig. 3). Other primary minerals present in the tailings include pyroxenes, andradite and axinite. Importantly, essentially no primary sulfides were detected using either bulk XRD or S near edge X-ray absorption fine structure (NEXAFS) spectroscopy (data not shown) in these surficial tailings, even when accounting for the smaller absorption cross section of sulfides. Oriented clay patterns (not shown) contain a strong peak at 1.0 nm d-spacing that is unchanged by saturation or heat treatment. This peak is observed in the silt and clay size fractions, but not in the sand fraction, suggesting that fine-grained mica (sericite) could be present and weathering to the clay mineral illite or another secondary clay. Support for the latter possibility is contributed by companion EXAFS studies, reported elsewhere (Hayes et al., 2009), that indicate the presence of Zn-talc, a secondary phase with 1.0 nm 001 d-spacing that has been identified in a variety of Zn-contaminated environments (Schlegel et al., 2001). This phase may not have sufficient long range order required for detection by XRD. Kaolinite, a common weathering product of feldspar, was also detected in $T_{4.2}$. Among the secondary sulfate phases, gypsum and jarosite were predominant (Fig. 3); both are common secondary phases in arid mine tailings systems (Jambor, 1994). Some rough pH trends in mineralogy are evident. In particular, with decreasing pH, abundances of andradite and axinite decrease, whereas those of orthoclase and jarosite increase.

4.3. Single and Sequential Extractions

The total mass and lability of contaminant metals in the tailings, as judged by total digests and sequential extractions, respectively, vary considerably with tailings pH (Table 3 and Fig. 4). For the purposes of this paper, the "labile" fraction is defined as that portion of the total metal pool that is soluble or exchangeable, i.e., extracted from the tailings during the water plus ammonium acetate steps of the sequential extraction. Additionally, the dissolution of the mineral phases targeted by each step of the sequential extraction was necessarily confirmed, as sequential extractions are operationally defined and do not necessarily completely and selectively dissolve only the target phase. For all tailings, most of the Al, Fe and Mn is immobile during the sequential extraction and is recovered in the residual fraction, whereas the Pb and Zn pools indicate greater lability (as measured by the fraction of each that is solubilized during the sequential extraction) (Fig. 4b). Large acid ammonium oxalate (AAO) 25°C and acid-extractable pools of Mn are present in the higher pH tailings. Most of the Fe appears to be residually-bound in primary silicates, but a significant fraction is also solubilized in the AAO 80°C extraction, targeting longer-range order Fe oxy(hydroxides) and jarosites.

The fractions of Pb and Zn released during sequential extraction are substantially greater than those for Al, Mn and Fe, although they are most often represented by lower total concentrations (Fig. 4b). This observation is consistent with the much higher values of DTPA extractable (i.e., bioavailable) Pb and Zn relative to Al, Mn and Fe (Fig. 1–Fig. 2). The tailings-bound Pb exhibits low water solubility (0–1.3%) in all samples. $T_{3.9}$ and $T_{5.4}$ contain larger acetic acid exchangeable fractions (17 and 33%, respectively) than $T_{2.6}$ and $T_{4.2}$ (2 and 4%, respectively). Only a small fraction of Pb is removed in the acid ammonium oxalate (AAO) extractions (8–18%), but a larger portion (7–36%) is extracted in the subsequent H_2O_2 extraction targeting supergene sulfides and organic matter. However, this large H_2O_2 extractable Pb pool appears to be an artifact of Pb-oxalate precipitation during the preceding steps, as discussed below. The

acid extraction also removes a significant fraction of Pb. This is particularly apparent in the case of $T_{2.6}$, where the jarosite does not dissolve in either AAO step, but does in the later acid extraction step, wherein 55% of the total Pb was removed (Fig. 4b).

Zinc has a larger extractable fraction than Pb for each sample, including a significant portion that is water soluble (0.6–37%) (Fig. 4 and Table 3). The acetic acid exchangeable fraction increases from 1% to 41%, with increasing pH. The higher pH tailings also have a larger fraction of Zn that is extractable in AAO at 25°C, whereas the low pH tailings have more Zn extracted in AAO at 80°C. The release of Zn in the AAO 80°C extraction is consistent with the presence of Zn in association with Fe (oxy)hydroxides at low pH, and this is supported by bulk EXAFS (Hayes et al., 2009). The residual fraction decreases with increasing pH (from 50% to 0). For the higher pH tailings, the mass sum of the sequentially-extracted Zn equals or slightly exceeds that measured in the total digestion such that a residual fraction is not detected.

4.4 X-ray Diffraction of Bulk Residues

The water and AAO 80°C extraction steps resulted in the most significant changes in XRD patterns, as illustrated here using $T_{3.9}$ as a representative example. Figure 5 includes only those patterns for which sequential extraction steps indicated the removal of pertinent XRD peaks. These diffractograms include those of (i) unextracted tailings, (ii) the difference diffractogram derived from subtracting water extracted from unextracted tailings, (iii) post-AAO 25°C reacted tailings, and (iv) residual tailings. Gypsum, removed in the water extraction, is evident in the unextracted tailings, but not the post-AAO 25°C pattern. Differential XRD indicates that gypsum is removed during the water extraction step; gypsum peaks are dominant in the difference diffractogram obtained by subtracting the pattern for post-water extraction from that obtained prior to water extraction. Likewise, jarosite is evidently removed during the AAO 80°C extraction because peaks for this phase remain following the AAO 25°C extraction step, but they are absent from the diffractogram following AAO 80°C extraction (not shown). Interestingly, this was not the case for $T_{2.6}$, where jarosite peaks were removed only after the acid extraction step. In any case, for all tailings, jarosite peaks were absent from the residual diffractogram (Fig. 5). Goethite and hematite, should also be dissolved in the AAO 80°C step, but their dissolution is difficult to discern using XRD or DXRD for bulk tailings because their strongest diffraction peaks are overlain by quartz peaks. Goethite and hematite were, however, readily identified in XRD of the clay size fraction (data not shown). Peaks in the diffraction pattern of the "residual" fraction show only silicate phases that resist the vigorous $KClO_3/HCl/HNO_3$ extraction.

4.5 X-ray Absorption Spectroscopy of Bulk Residues

A detailed discussion of tailings EXAFS data analysis is outside the scope of this paper and is the subject of a companion manuscript (Hayes et al., 2009). However, of direct relevance to the current study are results that indicate an important artifact during the sequential extraction of Pb. To assess this effect, bulk Pb L_{III} edge EXAFS measurements were performed as part of this study, on solid-phase residues from the sequential extraction.

In unextracted tailings, Pb speciation is dominated by plumbojarosite, along with smaller amounts of AA-soluble anglesite, and adsorbed species (Hayes et al., 2009). However, all tailings, particularly the 3 higher pH samples, exhibit a dramatic change in the Pb L_{III} edge EXAFS spectra following AAO 80°C extraction (Fig. 6). The minimum of the indicator function from principal components analysis (Wasserman et al., 1999) indicates that the 8 spectra (unextracted and post AAO 80°C) can be adequately described with only two components. Additionally, target transform of plumbojarosite and Pb-oxalate (PbC_2O_4) reference spectra low SPOIL values, (2.4 and 4.1 for Pb oxalate and plumbojarosite, respectively) indicating that both are likely components of the sample spectra (Manceau et al.,

2002). Hence, the spectral change observed corresponds to the dissolution of plumbojarosite (which is targeted by the AAO80°C extraction) followed by the precipitation of PbC_2O_4, an oxalate solid that exhibits low water solubility (log $K_{sp}= -8.07$) (Skoog et al., 1996). Spectra for all tailings indicate that some fraction of Pb re-precipitates as PbC_2O_4, with $T_{2.6}$ showing the lowest fractional conversion (Fig. 6). This observation is consistent with the XRD results showing that jarosite was not effectively solubilized in $T_{2.6}$ until the acid extraction. In all cases, the oxidation of oxalate by H_2O_2 after the AAO reaction solubilizes the Pb that was retained in PbC_2O_4, such that subsequent release represents the mass precipitated as PbC_2O_4 (Fig. 4b). Therefore, this pool of Pb can not be assigned to native organically-bound Pb, or supergene Pb sulfides, which are the phases that are targeted by the H_2O_2 extraction step. The very low organic C contents of the tailings (Table 1) and the lack of XRD (Table 2) or Sulfur NEXAFS (data not shown) detectable sulfides are consistent with this conclusion.

4.6 Particle-Scale Elemental Mapping and Identification

Individual grains enriched in Pb or Zn were identified in micro-focused X-ray fluorescence (μ-XRF) mapping of thin sections, and subsequently probed using micro-focused Raman spectroscopy (μ-Raman) for phase identification. Representative elemental XRF maps are shown in Figure 7 and Figure 8 for $T_{2.6}$ and $T_{4.2}$, respectively. The XRF maps reveal clear elemental correlations that were frequently observed between contaminant metals and framework elements. In both figures, the correlation plots indicate that Pb is consistently collocated with S and Fe, but that both Fe and S also occur in particles with low Pb counts. Zinc is clearly collocated with Mn in $T_{4.2}$, but gives low counts in $T_{2.6}$. The same particles imaged using μ-XRF were also probed using μ-Raman in order to identify the specific mineral phase of contaminant-containing particles. These grains are identified in the μ-XRF maps of Figure 7a and Figure 8a, and the corresponding Raman spectra are shown in Figure 7c and Figure 8c. It is worth noting that the presence of most of the phases identified using bulk XRD were confirmed at the particle scale with μ-Raman (Table 2).

Correlation of Pb-Fe counts in $T_{2.6}$ (Fig. 7b) indicates 3 different populations for 3 different locations, spots 1–3, each corresponding to a discrete particle or aggregate indicated on the XRF map (Fig. 7a). A low Fe, high Pb, high S aggregate was identified as plumbojarosite (Fig. 7, spot 1), and a high Fe, low Pb particle was identified as hematite (Fig. 7, spot 2). Unfortunately, the high Fe, high Pb particle (Fig. 7, spot 3) sustained thermal damage before it could be identified. $T_{4.2}$ shows similar Pb-Fe correlation, including collocation of Pb, Fe and S in plumbojarosite aggregate (Fig. 8, spot 7). The other Fe-rich particles in Figure 8 have been identified as goethite.

Zinc is clearly collocated with Mn in all tailing samples, except in $T_{2.6}$, where both Zn and Mn total concentrations were substantially lower (Fig. 2a). The Zn-Mn collocations occur as reaction rinds on pyroxene particles (e.g. Fig. 8a, spot 11) or in particles represented by large aggregates (Fig. 8a, spots 12–13) that contain hedenbergite, johannsenite, and andradite in a matrix of manjiroite (e.g. spot 12), which apparently acts as a sorbent for Zn. At low pH, the Zn has a strong correlation with iron (Fig. 7b), indicating the possible re-adsorption of Zn to Fe oxides after dissolution of the Mn-oxides (Fig. 7a and c, spot 6).

5. Discussion

5.1 Role of Parent Mineral Weathering

The Klondyke tailings samples range in pH from 2.6 to 5.4, but several other physical and chemical properties are similar, which allows for a comparison of the relationship between sample pH and geochemical composition (Table 1–Table 2). The tailings primary minerals are expected to weather in a manner consistent with previously described weathering series

(Goldich, 1938;Reiche, 1950;Loughnan, 1969;Sverdrup, 1990;Velbel, 1999), listed here in order of presumed decreasing dissolution rate for this particular site: sulfides (galena, sphalerite, pyrite), calcite, andradite, axinite, pyroxenes (hedenbergite and johannsenite), K-feldspars (orthoclase), and quartz. In this progression, sulfide weathering is accompanied by a drop in pH (buffered by carbonate dissolution if present), and by secondary sulfate and oxide mineral precipitation or translocation of ions (Hudson-Edwards et al., 1996).

Nesosilicate, cyclosilicate and chain silicates are expected to weather before feldspars, and they are an important source of Fe, Mn and Ca to the system (Huang, 1989). Hence, the fact that andradite (nesosilicate) and axinite (cyclosilicate) are most prevalent in $T_{5.4}$ suggests that silicates in this tailing sample have undergone the least weathering (Sverdrup, 1990). Despite no noticeable difference in the relative amount of pyroxenes from XRD (Fig. 3), the relative enrichment of andradite and axinite in high pH tailings, and of orthoclase and jarosite in low pH tailings, suggests that the extent of tailings weathering increases with decreasing pH.

Most of the Fe in the tailings survives into the residual fraction containing the Fe silicates andradite, axinite and hedenbergite (Fig. 5). The extractable mass of Fe is primarily from the AAO 80°C step that targets crystalline Fe (oxy)hydroxides (goethite, hematite) and Fe (hydroxy)sulfates (jarosite, plumbojarosite). The one exception to this trend is with $T_{2.6}$, where (according to XRD results) the final HNO_3 acid extraction step was the one that dissolved, in this case, well-crystallized jarosite that survived the AAO extractions, resulting in a large release of Fe and Pb (Fig. 4). The highly-crystalline character of the jarosite and substantial release of Fe in the AAO 80°C extraction suggest that $T_{2.6}$ has been subjected to the greatest weathering extent. The aqueous geochemical conditions in $T_{2.6}$ (pH=2.6, $[SO_4]$=5.9 g kg^{-1} as depicted in Table 1) favor jarosite stability; its precipitation is mediated bacterially at pH < 2.5 with SO_4 concentrations greater than 3 g kg^{-1} (Bigham et al., 1996;Bigham and Nordstrom, 2000;Lottermoser, 2003). Iron weathers from the primary sulfide and silicate phases (pyrite, andradite, Fe-axinite and hedenbergite) to jarosite, plumbojarosite, goethite and hematite. The secondary Fe sulfates and (oxyhydr)oxides, in particular, are high affinity sinks for toxic metals and their formation in the Klondyke tailings appears to be an excellent sequestration mechanism for Pb^{2+} ions released during primary sulfide dissolution.

Total Mn in the tailings is found to decrease with decreasing pH, suggesting that a portion is lost due to weathering-induced translocation (Table 3 and Fig. 4a). This trend is mirrored in the initial sampling that shows that DTPA-extractable Mn decreases with progression to lower pH (Fig. 2). Whereas the residual Mn fraction increases with acidification, the total pool of residual Mn decreases (Table 3). These data suggest the preferential dissolution of more soluble Mn-bearing phases during weathering. Specifically, the mixed valence Mn oxides, manjiroite and chalcophanite, present in the higher pH samples, contribute to the substantial mass of Mn extracted by AAO at 25°C (Fig. 4b). Thus, while johannsenite and Mn-axinite weather to chalcophanite and manjiroite, these phases are only metastable and they are subjected to dissolution and leaching loss with further weathering. As suggested by the μ-XRF and μ-Raman data, these intermediate Mn-oxide phases can act as effective sinks for Zn that is released from sphalerite weathering, thereby reducing its lability.

In summary, trends in mineral prevalence and metal extractability suggest that the pH variation in the Klondyke surface tailings represents a weathering gradient, with the pH decline signaling time-progressive tailing acidification. Evidence to support this assertion includes the following results discussed above: (i) presence of carbonate only in $T_{4.2}$, (ii) depletion of gangue neso- and cyclo-silicates (andradite and axinite) with increased tailings acidification, (iii) persistence at low pH of kinetically-stable orthoclase and quartz relative to more soluble silicates, (iv) accumulation of kaolinite in $T_{4.2}$; (vi) accumulation of well-crystallized jarosite; and,

importantly, (vii) decreasing lability of both Pb^{2+} and Zn^{2+}. This latter effect is discussed in more detail in the following section.

5.2. Consequences for Contaminant Metal Lability

For Pb and Zn, elemental correlations with Fe and Mn, respectively, have been observed both at the field scale and at the particle scale (Fig. 1–Fig. 2, Fig. 7–Fig. 8). The source of these correlations relates directly to the weathering trajectories described above.

Lead is effectively sequestered into plumbojarosite, which becomes increasingly stable, and whose crystallinity increases, as weathering progresses, to more acidic pH. As a result of this effective sequestration, total Pb concentrations are not diminished over the course of mineral weathering in the tailings piles. The increasing recalcitrance of Pb in sulfate solids is consistent with the sequential extraction data that show a progressively larger fraction of Pb is incorporated into well-cystallized jarosite (and/or Fe oxyhydroxide) solids that are generally dissolved in the AAO80°C extraction steps (as indicated by XRD), but not until the acid extraction step for the most acidified sample, $T_{2.6}$. This influence of tailings pH on the speciation of Pb is reflected in the progressive growth of the fraction extracted by the sum of AAO80°C, H_2O_2 and acid extraction steps. As pointed out earlier, since Pb extracted by AAO80°C precipitates to form Pb-oxalate solids that are solubilized in the H_2O_2 step (Fig. 5), it is contended that the sum of the AAO and H_2O_2 extraction steps provides an estimate of Pb mass associated with Fe sulfate and (oxyhydr)oxide solids. Since plumbojarosite stability and crystallinity increases with decreasing pH, this suggests that Pb lability has decreased with increased weathering of the tailings piles. One measureable indication of this is that the water-extractable Pb decreases by a factor of 40 from $T_{5.4}$ to $T_{2.6}$ while total Pb decreases only by a factor of 4.

EXAFS results also indicate that a low recovery of Pb in oxalate extractions does not necessarily imply a low mass abundance of oxalate soluble mineral solids. In the case of Pb, not all trends in speciation can be related to pH variation alone, and a depth dependence in Pb lability is apparent. Tailings taken from the 0–30 cm depth ($T_{3.9}$ and $T_{5.4}$) both show larger acetic acid (AA) extractable pools relative to those sampled from the 28–53 cm and 21–42 cm depths ($T_{2.6}$ and $T_{4.2}$, respectively), which suggests a more labile (e.g., exchangeable) form of Pb is present in these surficial tailings.

Total Zn concentration decreases by roughly an order of magnitude with decreasing pH (Fig. 2a). A significant fraction of Zn is extracted by AAO (Fig. 4b), which dissolves the Mn oxides chalcophanite and manjiroite. That is, weathering of Mn-bearing silicate (axinite, johannsenite) phases gives rise to Mn oxides that effectively sequester Zn in co-precipitates (chalcophanite) or in high affinity sorption complexes (manjiroite). However, these solids are metastable in the tailings environment, and their loss from the tailings matrix seems to result in a concurrent leaching loss of Zn from the solid phase. Some of the Zn is scavenged by Fe (oxy)hydroxides, which are persistent in the low pH tailings. In addition, solid phase speciation of Zn likely includes a Zn-talc phase, whose presence is suggested by the contribution of a unique component to the Zn K-edge EXAFS spectra, as discussed in a companion paper (Hayes et al., 2009).

6. Conclusions

This study shows that weathering-induced acidification of highly-oxidized desert tailings can affect the solubility dynamics of residual metal mass. Lead partitions primarily into plumbojarosite aggregates, and since plumbojarosite is favored by low pH and high dissolved SO_4 conditions, the jarosite-bound Pb appears to become increasingly recalcitrant with tailings acidification coincident with increasing crystallinity of the jarosite host phase.

The mobility and fate of Zn appears coupled to the weathering of Mn-bearing solids. In particular, Mn(II) primary silicates, johannsenite and Mn-axinite, weather incongruently to form mixed valence Mn oxides, manjiroite and chalcophanite. These secondary products seem to act as high affinity sinks for Zn. The prevalence of these mixed-valence Mn solids decreases with decreasing tailings pH. This likely explains the correlated decrease in total Zn concentration and the possible sorption of Zn to Fe (oxy)hydroxides at low pH. Whereas the DTPA and sequential extraction results show a decrease in the labile fraction and pool size of Zn with increased tailings acidification, the total concentration of both Mn and Zn also decrease with acidification, suggestive of their leaching loss during weathering.

Acknowledgments

References

Alvarenga P, Palma P, Goncalves AP, Fernandes RM, de Varennes A, Vallini G, Duarte E, Cunha-Queda AC. Evaluation of tests to assess the quality of mine-contaminated soils. Environ. Geochem. Health 2008;30:95–99. [PubMed: 18246433]

Amacher, M. Nickel, cadmium and lead. In: Bartels, JM., editor. Methods of Soil Analysis Part 3: Chemical Methods. Madison, WI: Soil Science Society of America; 1996. p. 754-756.

Arai Y, Lanzirotti A, Sutton S, Davis JA, Sparks DL. Arsenic speciation and reactivity in poultry litter. Environ. Sci. Technol 2003;37:4083–4090. [PubMed: 14524439]

Bernaus A, Gaona X, Esbri JM, Higueras P, Falkenberg G, Valiente M. Microprobe techniques for speciation analysis and geochemical characterization of mine environments: The mercury district of Almaden in Spain. Environ. Sci. Technol 2006;40:4090–4095. [PubMed: 16856721]

Bigham, JM.; Nordstrom, DK. Iron and aluminum hydroxysulfates from acid sulfate waters. In: Alpers, CN.; Jambor, JL.; Nordstrom, DK., editors. Sulfate Minerals - Crystallography, Geochemistry and Environmental Significance. Vol. Vol. 40. Mineralogy & Geochemistry; 2000. p. 351-403.Reviews in

Bigham JM, Schwertmann U, Traina SJ, Winland RL, Wolf M. Schwertmannite and the chemical modeling of iron in acid sulfate waters. Geochim. Cosmochim. Acta 1996;60:2111–2121.

Blowes, DW.; Ptacek, CJ.; Jambor, JL.; Weisner, CG. The geochemistry of acid mine drainage. In: Lollar, BS., editor. Environmental Geochemistry. Vol. 9, Holland, H.D., Turekian, K.K. (Exec. Eds), Treatise on Geochemistry. Oxford: Elsevier–Pergamon; 2005. p. 149-204.

Burt, R. Soil physical and fabric-related analyses. In: Burt, R., editor. Soil Survey Laboratory Methods Manual. Soil Survey Investigations Report. National Resources Conservation Service; 2004. p. 34-43.

Calmano W, Mangold S, Welter E. An XAFS investigation of the artefacts caused by sequential extraction analyses of Pb-contaminated soils. Fresenius J. Anal. Chem 2001;371:823–830. [PubMed: 11768472]

Choi S, Crosson G, Mueller KT, Seraphin S, Chorover J. Clay mineral weathering and contaminant dynamics in a caustic aqueous system. II. Mineral transformation and microscale partitioning. Geochim. Cosmochim. Acta 2005;69:4437–4451.

Chorover J, Choi S, Rotenberg P, Serne RJ, Rivera N, Strepka C, Thompson A, Mueller KT, O'Day PA. Silicon control of strontium and cesium partitioning in hydroxide-weathered sediments. Geochim. Cosmochim. Acta 2008;72:2024–2047.

Courtin-Nomade A, Soubrand-Colin M, Marcus MA, Fakra SC. Evidence for the incorporation of lead into barite from waste rock pile materials. Environ. Sci. Technol 2008;42:2867–2872. [PubMed: 18497136]

Davis A, Drexler JW, Ruby MV, Nicholson A. Micromineralogy of mine wastes in relation to lead bioavailability, Butte, Montana. Environ. Sci. Technol 1993;27:1415–1425.

Dold B. Dissolution kinetics of schwertmannite and ferrihydrite in oxidized mine samples and their detection by differential X-ray diffraction (DXRD). Appl. Geochem 2003a;18:1531–1540.

Dold B. Speciation of the most soluble phases in a sequential extraction procedure adapted for geochemical studies of copper sulfide mine waste. J. Geochem. Explor 2003b;80:55–68.

Dold B, Fontbote L. Element cycling and secondary mineralogy in porphyry copper tailings as a function of climate, primary mineralogy, and mineral processing. J. Geochem. Explor 2001;74:3–55.

Downs, RT. The RRUFF Project: an integrated study of the chemistry, crystallography, Raman and infrared spectroscopy of minerals. Prog. Abstr. 19th General Meeting of the Internat. Mineralogical Association in Kobe; Japan. 2006. p. O03-O13.

Filippi M, Dousova B, Machovic V. Mineralogical speciation of arsenic in soils above the Mokrsko-west gold deposit, Czech Republic. Geoderma 2007;139:154–170.

Finzgar N, Tlustos P, Lestan D. Relationship of soil properties to fractionation, bioavailability and mobility of lead and zinc in soil. Plant Soil Environ 2007;53:225–238.

Goldich SS. A study in rock-weathering. J. Geol 1938;46:17–58.

Goodwin, SD. Preliminary Assessment/ Site Inspection Report: Klondyke Tailings. Phoenix, AZ: Arizona Department of Environmetal Quality; 2000.

Grandlic CJ, Mendez MO, Chorover J, Machado B, Maier RM. Plant growth-promoting bacteria for phytostabilization of mine tailings. Environ. Sci. Technol 2008;42:2079–2084. [PubMed: 18409640]

Hall GEM, Vaive JE, Beer R, Hoashi M. Selective leaches revisited, with emphasis on the amorphous Fe oxyhydroxide phase extraction. J. Geochem. Explor 1996;56:59–78.

Hayes SM, Bargar JR, Webb SM, Chorover J. Spectroscopic investigation of lead and zinc speciation in sulfate dominated arid mine tailings in Aravaipa Canyon, Arizona. 2009 In prep.

Huang, PM. Feldspars, Olivines, Pyroxenes, and Amphiboles. (Chapter 20). In: Dixon, JB.; Weed, SB., editors. Minerals in Soil Environments. Madison, WI: Soil Science Society of America; 1989. p. 975-1050.

Hudson-Edwards KA, Macklin MG, Curtis CD, Vaughan DJ. Processes of formation and distribution of Pb-, Zn-, Cd-, and Cu-bearing minerals in the Tyne Basin, northeast England: Implications for metal-contaminated river systems. Environ. Sci. Technol 1996;30:72–80.

Hudson-Edwards KA, Schell C, Macklin MG. Mineralogy and geochemistry of alluvium contaminated by metal mining in the Rio Tinto area, southwest Spain. Appl. Geochem 1999;14:1015–1030.

Jackson, ML. Soil Chemical Analysis. Madison, Wisconsin: Parallel Press; 1985.

Jambor, JL. Mineralogy of Sulfide-rich Tailings and Their Oxidation Products. (Chapter 3). In: Jambor, JL.; Blowes, DW., editors. The Environmental Geochemistry of Sulfide Mine-wastes. Vol. Vol. 22. Mineral. Assoc. Can., Short Course; 1994. p. 59-102.

Jeong GY, Lee BY. Secondary mineralogy and microtextures of weathered sulfides and manganoan carbonates in mine waste-rock dumps, with implications for heavy-metal fixation. Am. Mineral 2003;88:1933–1942.

Johnson RH, Blowes DW, Robertson WD, Jambor JL. The hydrogeochemistry of the Nickel Rim mine tailings impoundment, Sudbury, Ontario. J. Contam. Hydrol 2000;41:49–80.

Lande, J.; Webb, SM.; Mehta, A. Area Diffraction Machine. 2007. http://groups.google.com.ezproxy2.library.arizona.edu/group/area-diffraction-machine

Lottermoser, BG. Mine Wastes: Characterization, Treatment, and Environmental Impacts. Berlin ; New York: Springer; 2003.

Loughnan, FC. Chemical Weathering of the Silicate Minerals. New York: American Elsevier Publishing Co; 1969.

Maiz I, Arambarri I, Garcia R, Millan E. Evaluation of heavy metal availability in polluted soils by two sequential extraction procedures using factor analysis. Environ. Pollut 2000;110:3–9. [PubMed: 15092851]

Manceau A, Marcus MA, Tamura N. Quantitative speciation of heavy metals in soils and sediments by synchrotron X-ray techniques. Applications of Synchrotron Radiation in Low-Temperature Geochemistry and Environmental Sciences 2002;49:341–428.

McCarty DK, Moore JN, Marcus WA. Mineralogy and trace element association in an acid mine drainage iron oxide precipitate; comparison of selective extractions. Appl. Geochem 1998;13:165–176.

McGregor RG, Blowes DW, Jambor JL, Robertson WD. The solid-phase controls on the mobility of heavy metals at the Copper Cliff tailings area, Sudbury, Ontario, Canada. J. Contam. Hydrol 1998;33:247–271.

Mendez MO, Maier RM. Phytostabilization of mine tailings in arid and semiarid environments - An emerging remediation technology. Environ. Health Perspect 2008;116:278–283. [PubMed: 18335091]

Mendez MO, Glenn ER, Maier RM. Phytostabilization potential of quailbush for mine tailings: Growth, metal accumulation, and microbial community changes. J. Environ. Qual 2007;36:245–253. [PubMed: 17215233]

Mendez MO, Neilson JW, Maier RM. Bacterial community characterization of a historic semiarid lead-zinc mine tailings site. Appl. Environ. Microbiol 2008;74:3899–3907. [PubMed: 18424534]

Navarro A, Collado D, Carbonell M, Sanchez JA. Impact of mining activities on soils in a semi-arid environment: Sierra Almagrera district, SE Spain. Environ. Geochem. Health 2004;26:383–393. [PubMed: 15719161]

O'Day PA, Carroll SA, Waychunas GA. Rock-water interactions controlling zinc, cadmium, and lead concentrations in surface waters and sediments, US Tri-State Mining District. 1. Molecular identification using X-ray absorption spectroscopy. Environ. Sci. Technol 1998;32:943–955.

Plumlee, GS.; Ziegler, TL. The medical geochemistry of dusts, soils and other earth materials. In: Lollar, BS., editor. Environmental Geochemistry. Vol. 9, Holland, H.D., Turekian, K.K. (Exec. Eds), Treatise on Geochemistry. Oxford: Elsevier–Pergamon; 2005. p. 263-310.

Reiche, P. A Survey of Weathering Processes and Products. Albequerque, NM: The University of New Mexico Press; 1950.

Ribet I, Ptacek CJ, Blowes DW, Jambor JL. The Potential for Metal Release by Reductive Dissolution of Weathered Mine Tailings. J. Contam. Hydrol 1995;17:239–273.

Romero FM, Armienta MA, Gonzalez-Hernandez G. Solid-phase control on the mobility of potentially toxic elements in an abandoned lead mine. Appl. Geochem 2007;22:109–127.

Schaider LA, Senn DB, Brabander DJ, McCarthy KD, Shine JP. Characterization of zinc, lead and cadmium in mine waste: Implications for transport, exposure and bioavailability. Environ. Sci. Technol 2007;41:4164–4171. [PubMed: 17612206]

Scheinost AC, Rossberg A, Marcus M, Pfister S, Kretzschmar R. Quantitative zinc speciation in soil with XAFS spectroscopy: Evaluation of iterative transformation factor analysis. Physica Scripta 2005;T115:1038–1040.

Schlegel ML, Manceau A, Charlet L, Chateigner D, Hazemann JL. Sorption of metal ions on clay minerals. III. Nucleation and epitaxial growth of Zn phyllosilicate on the edges of hectorite. Geochim. Cosmochim. Acta 2001;65:4155–4170.

Schulze, DG. Differential X-ray diffraction analysis of soil minerals. (Chapter 13). In: Amonette, JE.; Zelany, LW., editors. Quantitative Methods in Soil Mineralogy. Madison, WI: Soil Science Society of America; 1994. p. 412-419.

Schuwirth N, Voegelin A, Kretzschmar R, Hofmann T. Vertical distribution and speciation of trace metals in weathering flotation residues of a zinc/lead sulfide mine. J. Environ. Qual 2007;36:61–69. [PubMed: 17215213]

Scott DC. Mineral Resources of the Aravaipa Study Area, Grahm and Pinal Counties. Arizona. MLA 1988:38–88.

Simons FS. Geology of the Klondyke quadrangle, Graham and Pinal Counties, Arizona. Geol. Surv. Prof. Paper 1964:461.

Skoog, DA.; Holler, FJ.; Nieman, TA. Principles of Instrumental Analysis. Chicago: Saunders College Publishing; 1998.

Skoog, DA.; West, DM.; Holler, FJ. Fundamentals of Analytical Chemistry. New York: Saunders College Publishing; 1996.

Sondag F. Selective Extraction Procedures Applied to Geochemical Prospecting in an Area Contaminated by Old Mine Workings. J. Geochem. Explor 1981;15:645–652.

Stefaniak EA, Worobiec A, Potgieter-Vermaak S, Alsecz A, Torok S, Van Grieken R. Molecular and elemental characterisation of mineral particles by means of parallel micro-Raman spectrometry and scanning electron microscopy. Spectrochim. A cta Part B-Atom. Spectrosc 2006;61:824–830.

Sumner, ME.; Miller, WP. Cation exchange capacity of soils containing salts, carbonates or zeolites. (Chapter 40). In: Sparks, DL., editor. Methods of Soils Analysis, Part 3: Chemical Methods. Madison, WI: Soil Science Society of America, Inc; 1996. p. 1201-1229.

Sverdrup, HU. The Kinetics of Base Cation Release Due to Chemical Weathering. Lund, Sweden: Lund University Press; 1990.

Tessier A, Campbell PGC, Bisson M. Sequential Extraction Procedure for the Speciation of Particulate Trace-Metals. Anal. Chem 1979;51:844–851.

Tummala, PSL.; Humble, W. Public Health Assessment: Klondyke Mine Tailings. Phoenix, AZ: Arizona Department of Health Services; 1998.

Vazquez-Ortega A, Hayes SM, Maier RM, Chorover J. Mobilization of lead and zinc in acid sulfate mine tailings buffered by gypsum dissolution. 2009 In prep.

Velbel MA. Bond strength and the relative weathering rates of simple orthosilicates. Am. J. Sci 1999;299:679–696.

Wasserman SR, Allen PG, Shuh DK, Bucher JJ, Edelstein NM. EXAFS and principal component analysis: a new shell game. J. Synchrot. Radiat 1999;6:284–286.

Webb SM. Sixpack: A graphical user interface for XAS analysis using IFEFFIT. Physica Scripta 2005;T115:1011–1014.

Webb, SM. Sam's Microprobe Analysis Tool Kit. 2006. http://www-ssrl.slac.stanford.edu/~swebb/smak.htm

Wray DS. The impact of unconfined mine tailings and anthropogenic pollution on a semi-arid environment - an initial study of the Rodalquilar mining district, south east Spain. Environ. Geochem. Health 1998;20:29–38.
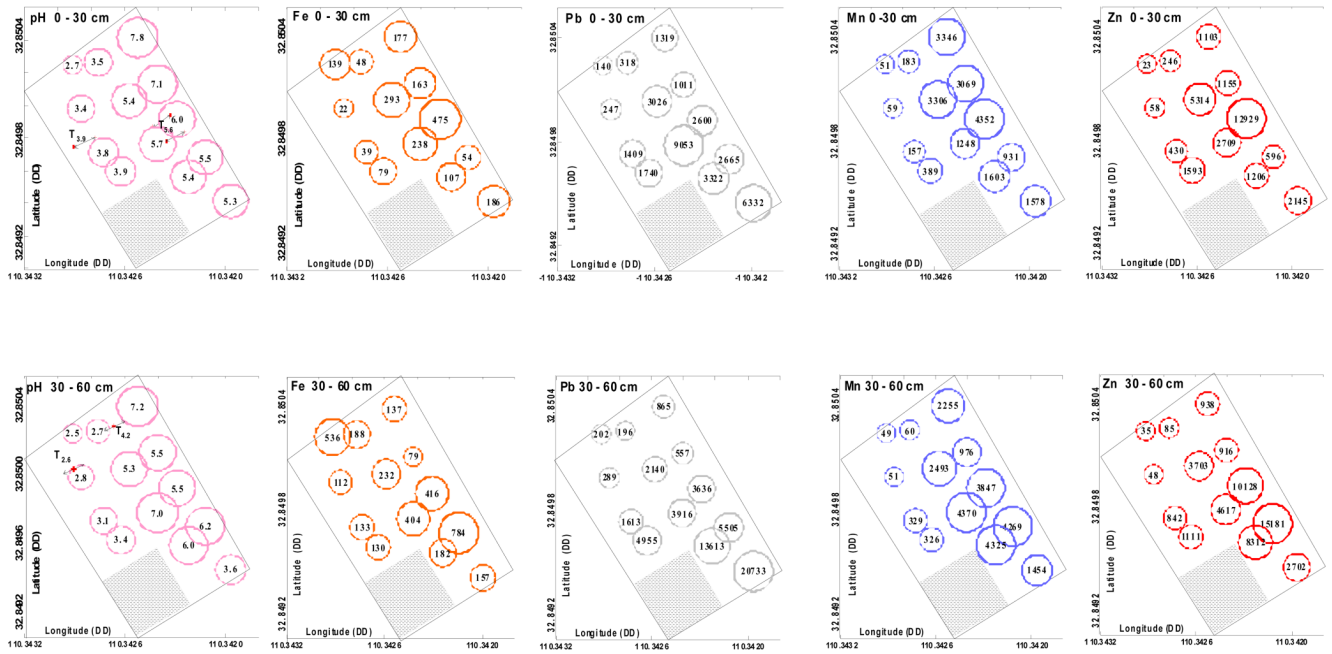
Figure 1.
Bubble plots of tailings piles for 0–30 cm depth (top row) and 30–60 cm depth (bottom row) from chemical data for sample locations shown as center of bubbles. Plots show (from left to right): saturated paste pH, and DTPA extractable metals (Fe, Pb, Mn and Zn, all in mg kg^{-1}) across the field site. Locations for sampling of T3.9 and T5.6 (sampled largely from within the 0–30 cm depth increment) are shown in the top pH graph, whereas locations for sampling of T2.6 and T4.2 (sampled largely from within the 30–60 cm depth increment) are shown in the bottom pH graph.
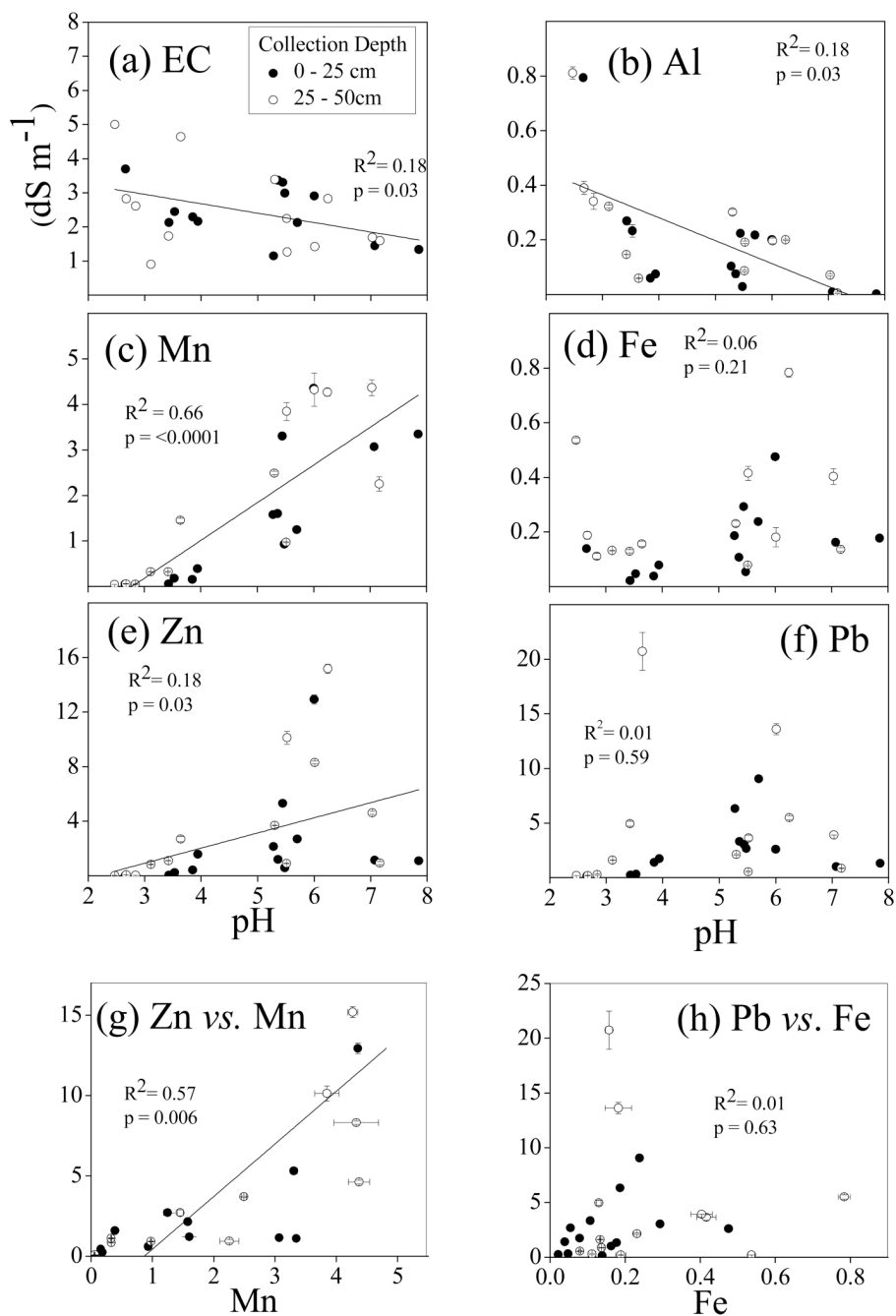
Figure 2.
Aqueous phase electrical conductivity (EC) and DTPA extractable metals from initial surface and subsurface sampling of tailings. (a) EC (in units of dS m^{-1}) versus tailings pH. In parts (b–f) DTPA extractable concentrations of various metals are plotted in units of grams of metal extracted/kg of tailings dry mass (g kg^{-1}), but note that each is plotted on its own Y axis scale versus a consistent X axis pH scale: (b) Al, (c) Mn, (d) Fe, (e) Zn, (f) Pb. Bottom two graphs show (g) Zn versus Mn, and (h) Pb versus Fe correlations in DTPA extracts (all in units of g kg^{-1}). Linear regression statistics are shown on each plot, but lines are shown only in cases where linear fits were statistically significant ($p < 0.05$).
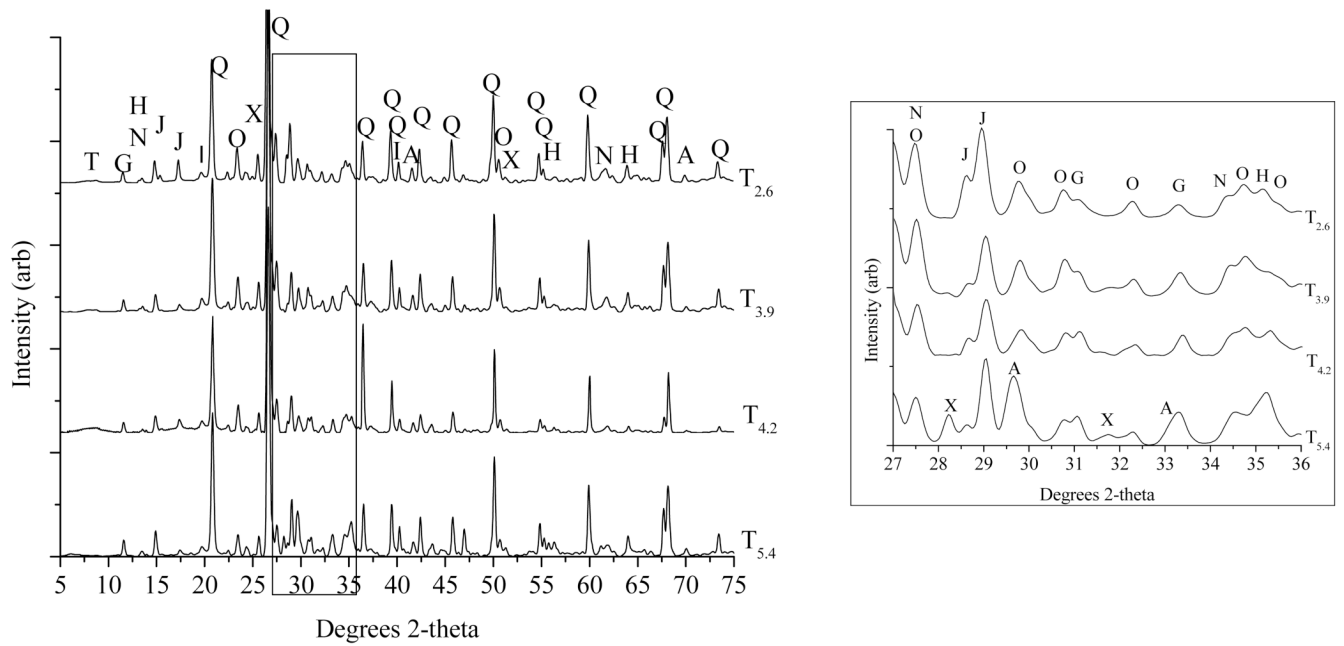
Figure 3.
X-ray powder diffraction patterns of tailings samples (< 2 mm fraction). Left side is full diffraction pattern, whereas right side shows expanded portion for 27–36 °2θ, which contains peaks corresponding to key silicate and sulfate phases. Phases identified, in order of relative abundance: quartz (Q), orthoclase (O), jarosite (J), gypsum (G), hedenbergite (H), johannsenite (N), Zn-talc (T), axinite (X), and andradite (A).

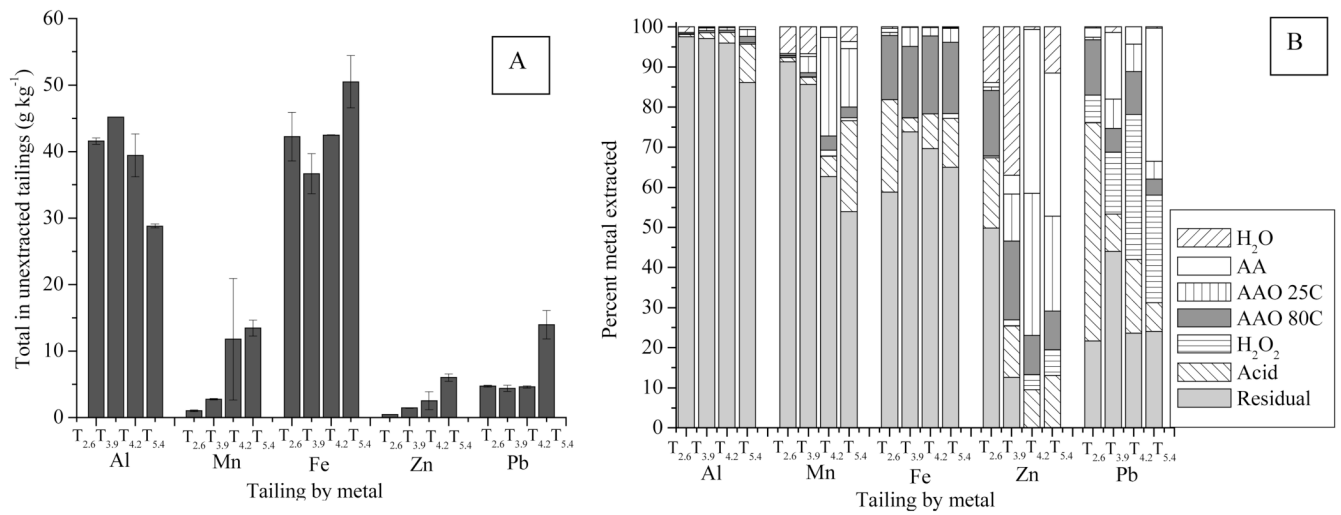**Figure 4.**
Total metal concentrations and partitioning. (A) Total metal concentrations in the 4 selected tailings samples (g kg^{-1}), (B) Fraction of each metal (relative to total) that is solubilized during each step of the sequential extraction.
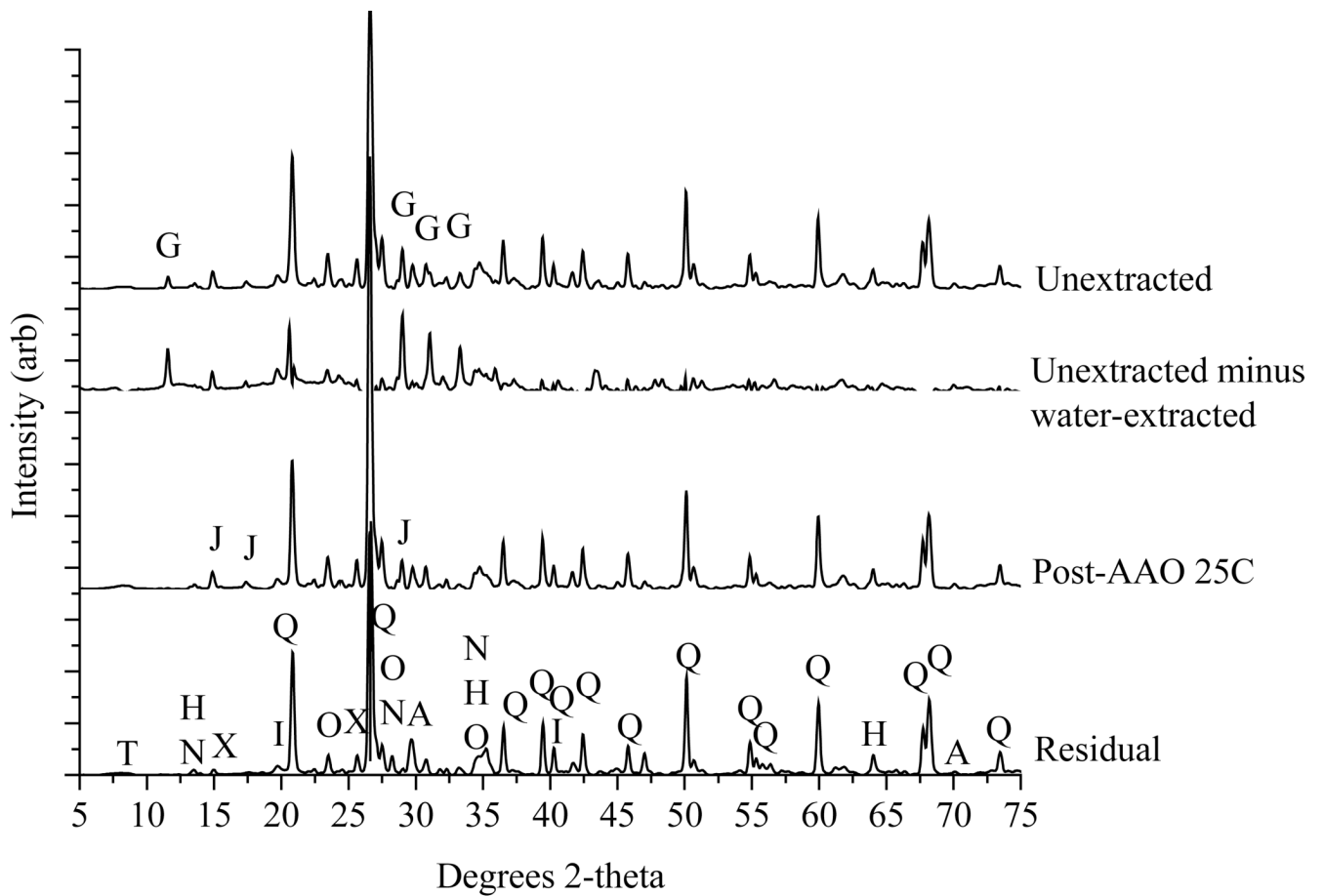
Figure 5.
X-ray diffraction patterns obtained after pertinent steps in the sequential extraction of $T_{3.9}$.
From top to bottom: (i) unextracted, (ii) unextracted minus water extracted, (iii) acid
ammonium oxalate extracted (25°C); (iv) residual. Gypsum (G) dissolves during the water
extraction, as shown by the difference diffractogram calculated from the patterns for
unextracted minus water-extracted solids. Jarosite (J) peaks shown in the post-AAO 25°C
pattern are removed during the subsequent extraction and are not present in the residual pattern,
indicating jarosite dissolution during the AAO 80°C step. Following the acid extraction, only
aluminosilicate phases remain. Minerals remaining after acid extraction include: quartz (Q),
orthoclase (O), hedenbergite (H), johannsenite (N), Zn-talc (T), axinite (X), and andradite (A).
Diffractograms for other extraction steps are not shown because there are no changes in the
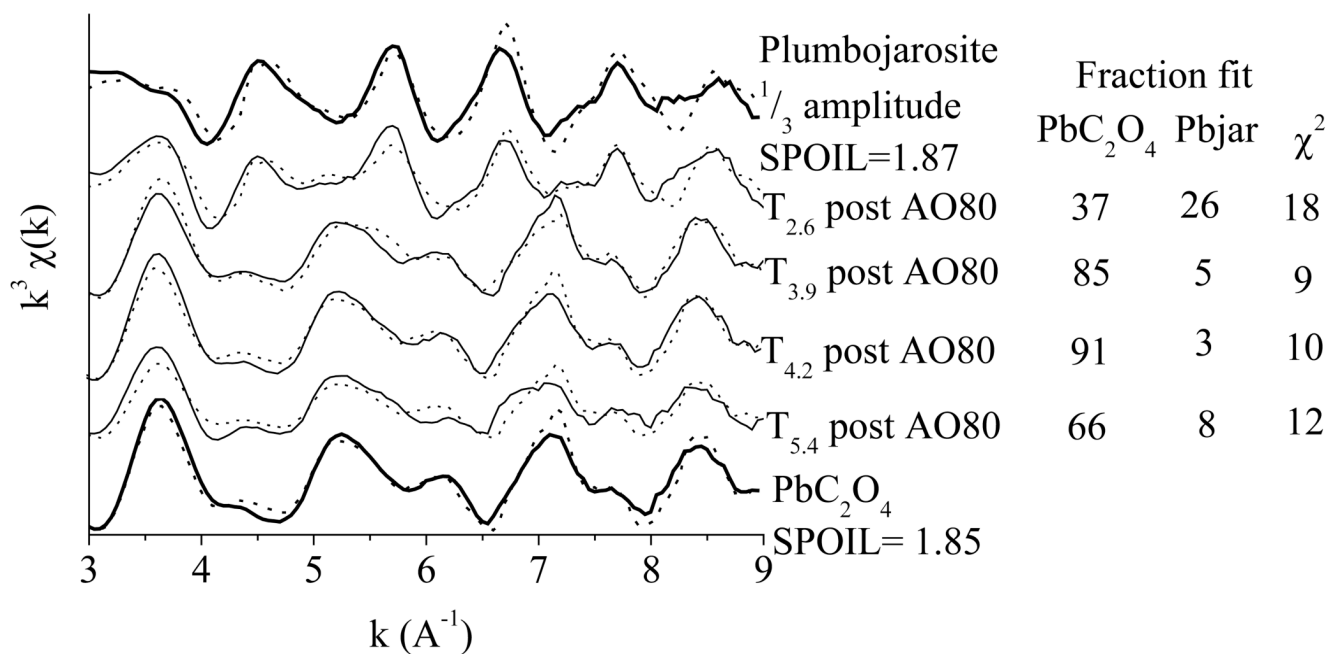pattern.

The table embedded within the figure:

	Fraction fit		
	PbC_2O_4	Pbjar	χ^2
$T_{2.6}$ post AO80	37	26	18
$T_{3.9}$ post AO80	85	5	9
$T_{4.2}$ post AO80	91	3	10
$T_{5.4}$ post AO80	66	8	12

Figure 6.
Formation of Pb-oxalate from plumbojarosite dissolution during the sequential extraction. Lead L_{III} edge EXAFS spectra of tailings samples after they have been subjected to high temperature, acid ammonium oxalate extraction (AAO80°C). Data are shown in solid lines and the linear combination fits (LCFs) using just two references (plumbojarosite and Pb-oxalate) are shown in dashed lines. Reference spectra are shown in bold with their mathematical reconstructions (dashed lines) from target transfer analysis, which was used to determine the suitability of the reference spectra for use in LCF.
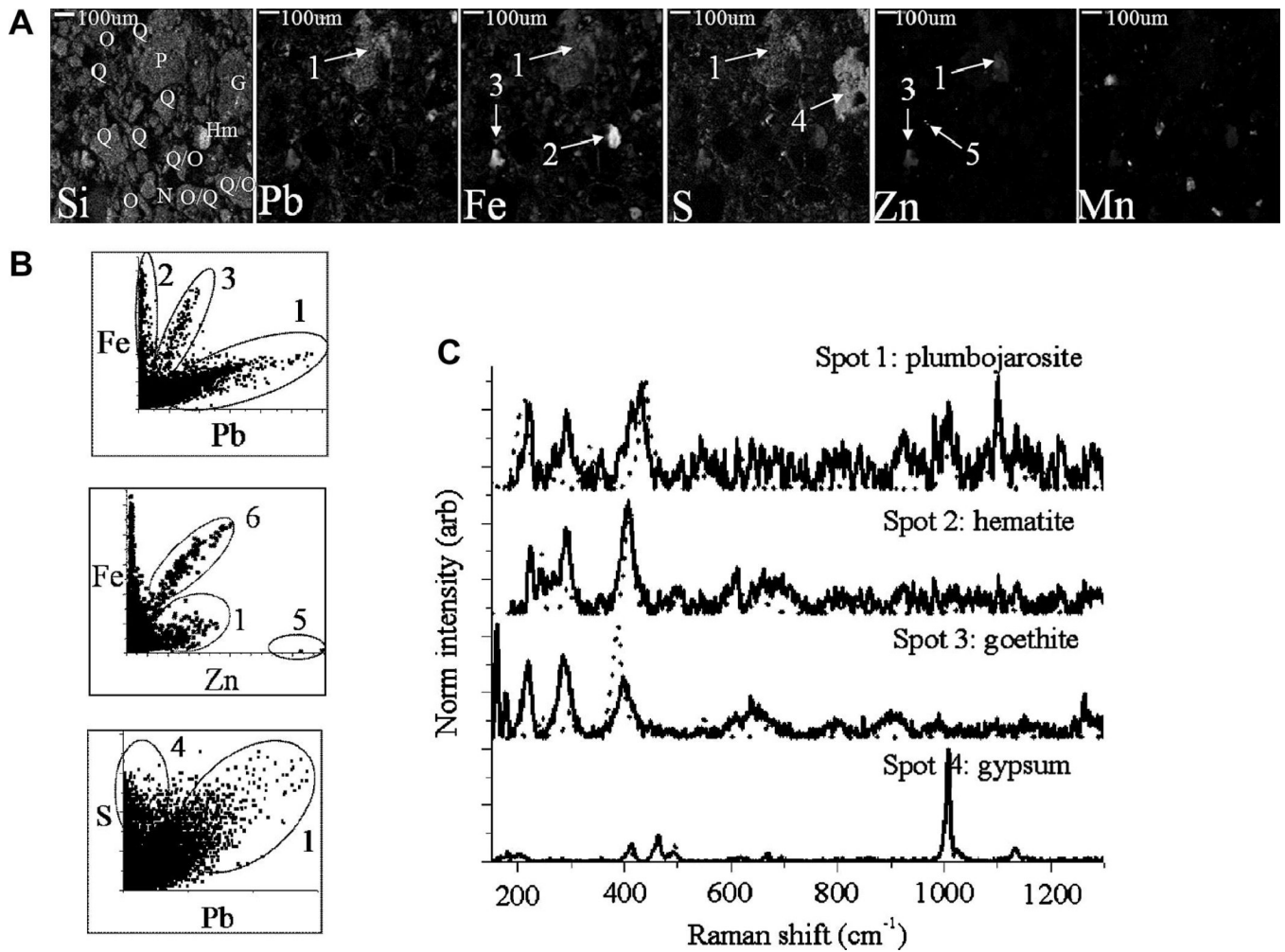
Figure 7.
Lead and Zn containing phases in $T_{2.6}$. (A) XRF map (see Table 2 for abbreviations of mineral in Si map), (B) Pb-Fe and Pb-S correlation plots from the XRF map, (C) Micro-Raman spectra showing grain-scale mineral phase identification (spectra shown in solid lines and RRUFF references shown in dotted lines).

Figure 8.
Lead and Zn containing phases in $T_{4.2}$. (A) XRF map (see Table 2 for abbreviations of mineral in Si map), (B) Pb-Fe, Pb-S and Zn-Mn correlation plots from the XRF map, (C) Micro-Raman spectra showing grain-scale mineral phase identification (spectra shown in solid lines and RRUFF references shown in dotted lines).
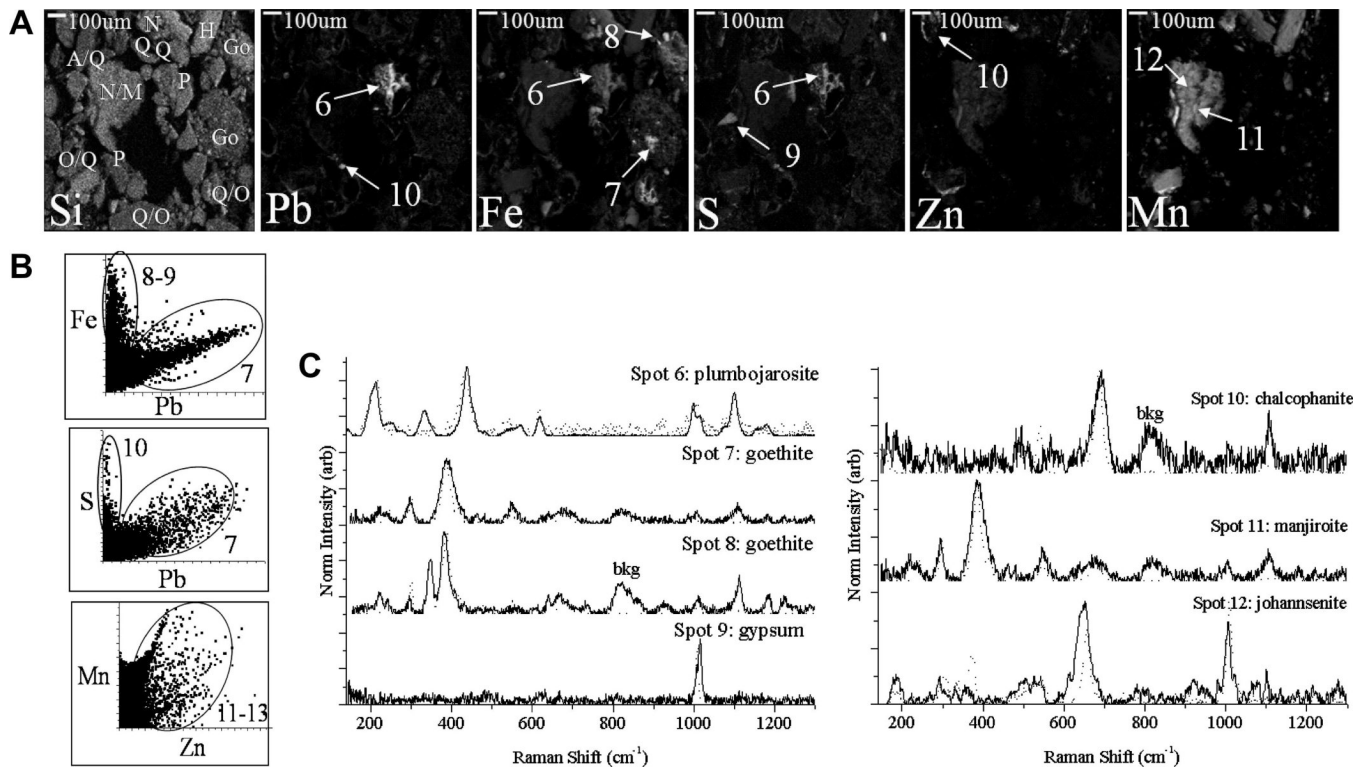
Table 1

Selected physical-chemical properties of the tailings selected for detailed study (std. dev. in parentheses).

	pH[a]	EC[a]	CEC[b]	SO$_4^{2-}$[a]	S$_{total}$[c]	TOC[d]	TIC[d]	TN[d]	Sand[e]	Silt[e]	Clay[e]
		mS cm^{-1}	cmol kg^{-1}	g S kg^{-1}	g kg^{-1}	mg kg^{-1}			percent		
T$_{2.6}$	2.61 (3)	5.6 (2)	21.7 (4)	5.9 (4)	23(5)	1380 (30)	<66	85 (2)	59.5 (2)	24.0 (5)	11 (1)
T$_{3.9}$	3.87 (6)	3.0 (1)	17 (3)	2.05(1)	16(1)	620 (40)	<66	65 (2)	50 (1)	33 (1)	7.9 (7)
T$_{4.2}$	4.22 (2)	3.2 (2)	17 (3)	2.34(6)	14.8(1)	400 (100)	590 (70)	37 (2)	62.6 (7)	19 (2)	11.1 (7)
T$_{5.4}$	5.44 (3)	3.49 (5)	23 (1)	2.4(5)	25()	940 (30)	<66	66 (2)	59.2 (7)	25 (1)	8 (1)

[a] Measured on a 1:1 solid to solution ratio 1 h extraction performed in triplicate.

[b] Measured using method developed for soils containing salts and carbonates (Sumner and Miller, 1996)

[c] Total elemental analysis on solid phase performed at Activation Laboratories by HCl, HNO3, HClO4, HF acid digestion-ICP.

[d] Solid state measurements on Shimadzu TOC-VCSH performed in triplicate.

[e] Measured in triplicate using the pipet method (Jackson, 1985).

Table 2

Mineral phases identified in the Klondyke tailings. Primary phases in bold, secondary phases in italics.

Phases	Formula	Abbreviation	Detection method[a]
andradite	$Ca_3Fe(III)_2(SiO_4)_3$	A	B-XRD, Raman
axinite	$Ca_2(Fe(II),Mn(II))Al_2BSi_4O_{15}(OH)$	X	B-XRD, Raman
hedenbergite	$CaFe(II)Si_2O_6$	H	B-XRD, Raman
johannsenite	$CaMn(II)Si_2O_6$	N	B-XRD, Raman
orthoclase	$K(AlSi_3)O_8$	O	B-XRD, Raman
quartz	SiO_2	Q	B-XRD, Raman
chalcophanite	$(Zn,Fe(II),Mn(II))Mn(IV)_3O_7 \cdot 3H_2O$	Ca	Raman
goethite	$FeO(OH)$	Go	Raman
gypsum	$CaSO_4 \cdot 2H_2O$	G	B-XRD, Raman
hematite	$Fe(III)_2O_3$	Hm	C-XRD, Raman
jarosite	$KFe(III)_3(SO_4)_2(OH)_6$	J	B-XRD, Raman
kaolinite	$Al_2Si_2O_5(OH)_4$	K	O-XRD
manjiroite	$(K,Na)(Mn(II),Mn(IV))_8O_{16} \cdot nH_2O$	M	Raman
plumbojarosite	$Pb(Fe(III)_3(SO_4)_2(OH)_6)_2$	P	Raman, XAS
Zn-Talc	$(Zn_{0.8}Mg_{0.2})_3Si_4O_{10}(OH)_2$	T	B-XRD, O-XRD

[a]Detection methods: Bulk XRD (B-XRD), oriented clay XRD (O-XRD), clay size fraction XRD (C-XRD), X-ray Absorption Spectroscopy (XAS), micro-focused Raman spectroscopy (Raman).

Table 3

Elemental content per unit mass of tailings: (i) total, (ii) water extracted, (iii) ammonium oxalate extracted (80°C), and (iv) residual fractions. Data included here (s.d. in parentheses) are based on sequential extraction steps with significant changes in the XRD pattern.

	K	Ca	Al	Si	Mn	Fe	Zn	Pb
Total elemental content in the unextracted tailings (g kg⁻¹) [a]								
$T_{2.6}$	76(3)	14.2(3)	41.5(4)	322(3)	1.1(1)	42(4)	0.45(2)	4.7(1)
$T_{3.9}$	67(1)	20(20)	45.2(0)	330(10)	2.7(1)	37(3)	1.43(5)	4.4(4)
$T_{4.2}$	59(7)	30(10)	39(3)	316(3)	12(1)	42.47(4)	3(1)	4.6(2)
$T_{5.4}$	39(1)	46(2)	28.7(3)	300(20)	13(1)	50(4)	6.0(6)	13.9(2)
Water, the first sequential extraction step (mg kg⁻¹)								
$T_{2.6}$	7(2)	0.56 (2)E3	570(30)	5(5)	70(10)	150(10)	60(10)	10(2)
$T_{3.9}$	100(6)	8.0(5)E3	44(2)	33(5)	180(50)	28(2)	530(20)	60(3)
$T_{4.2}$	60(10)	6.3(6)E3	1.0 (6)	9 (10)	3.9(3)	0.5(2)	23(3)	0.02(1)
$T_{5.4}$	700(300)	10.(4)E3	5(2)	12000(200)	400(2)	400(10)	700(300)	400(20)
Sequential extraction step: ammonium oxalate 80°C (mg kg⁻¹)								
$T_{2.6}$	1.3(2)E3	0.01(1)E2	0.067(7)E2	1.6(2)E2	0.05(5)E2	6.8(5)E3	0.73(5)E2	6.6(9)E2
$T_{3.9}$	0.6(3)E3	8(4)E2	2(2)E2	4.7(6)E2	0.30(1)E2	7(3)E3	3(1)E2	3(1)E2
$T_{4.2}$	1.1(7)E3	0.6(1)E2	2.2(1)E2	11(4)E2	4.2(2)E2	8.3(7)E3	4(1)E2	5(1)E2
$T_{5.4}$	1.41(6)E3	10(1)E2	5.0(4)E2	14.2(9)E2	3.6(5)E2	9(1)E3	6.2(5)E2	5(2)E2
Residual elements after acid extraction (g kg⁻¹) [b,c]								
$T_{2.6}$		7.1(5)	40.5(5)	321(3)	0.9(1)	25(4)	0.22(2)	1.0(2)
$T_{3.9}$		7(2)	43.9(1)	330(10)	2.3(1)	27(4)	0.2(1)	2.0(5)
$T_{4.2}$		20(1)	38(3)	312(3)	74(9)	29.6(8)	0[c]	1.0(3)
$T_{5.4}$		19(5)	24.8(3)	300(20)	73(1)	33(4)	0[c]	3.2(4)

[a] Total elemental analysis performed at Activation Laboratories. Most of the elements listed here were quantified using a Li metaborate/tetraborate fusion, followed by ICP-OES or ICP-MS analysis. HCl, HNO3, HClO4, HF acid digestion-ICP.

[b] KClO4 is used as a reagent in the acid extraction. Thus it is not possible to quantify the residual K content.

[c]For the two higher pH samples, the sum of Zn mass extracted in all sequential extraction steps was equal to, or slightly exceeded, that measured in the total elemental analysis. Hence, no residual Zn was detected for these samples.